# Numerical investigation of the aeroacoustic properties of a slot diffuser

*Lisa* Krüger[1*], *Philipp* Ostmann[1], *Martin* Kremer[1] and *Dirk* Müller[1]

[1]Institute for Energy Efficient Buildings and Indoor Climate, RWTH Aachen University, Germany

**Abstract.** Reducing noise emissions from building ventilation systems not only improves acoustic comfort but also extends the operating limits of mechanical ventilation systems. The geometric characteristics of an air diffuser have a significant influence on its acoustic behavior. Implementing geometric modifications early in the design process based on a simulation model offers a promising approach for optimization. This paper introduces a numerical model of a commercial slot diffuser. The study aims to investigate the applicability of aeroacoustic simulation for deriving noise reduction strategies by the successful prediction of acoustic characteristics. We compute the acoustic pressure below the diffuser within a Large Eddy Simulation (LES) in combination with an approach based on the Linearized Perturbed Compressible Equations (LPCE). Acoustic measurements are performed to verify the transient simulation solution. A comparison of the power spectral densities obtained from the experiment and simulation confirms that the model successfully reproduces the characteristic properties of the commercial air diffuser at the investigated operating points. Limitations arise from insufficient resolution in the low-frequency range due to the short time interval considered and external influences on the acoustic measurements. With the aim of noise reduction, we implement modifications in the form of droplet-shaped elements at a leading edge of the air diffuser geometry and investigate their influence on the acoustic behavior of the air diffuser.

## 1 Introduction

The strengthening emphasis on energy-efficient buildings, healthy indoor air quality, and stricter regulatory requirements for building air tightness [1] lead to a steadily increasing number of buildings equipped with mechanical ventilation. As a result, the sound emissions generated by ventilation units are also gaining greater significance in the context of user acceptance. The ventilation unit's sound emission is closely linked to the supply volume flow rate as well as the perceived acoustic comfort since the allowed noise level of an air diffuser constrains the maximum supply volume flow rate. Decreasing an air diffuser's sound emission simultaneously improves acoustic comfort and broadens the system's operating limits. It enables the ventilation system to provide the required thermal capacity through a higher volume flow rate while decreasing the temperature difference between supply and room air. In consequence, an implemented refrigeration unit can operate at a more efficient point.

Noise within the airflow results from forces acting on the flow surfaces. These forces arise in unsteady flows due to turbulence in zones with flow separation and reversed flow around sharp edges and shear layers because of high-velocity gradients [2]. The Navier-Stokes equations capture these aeroacoustic phenomena. Consequently, numerical equations can describe noise generation and propagation by analogy. Acoustic analogies provide reliable results with relatively low computational effort in flow regions where a minimal dynamic pressure component is present. However, hybrid models are required to resolve acoustic phenomena in regions of strong turbulent fluctuations [3]. In this work, we apply an approach based on the Linearized Perturbed Compressible Equations (LPCE) to calculate and investigate the acoustic pressure emitted by the slot diffuser.

Numerical aeroacoustics offer the opportunity to comprehend the influence of geometric features on noise generation, allowing for their precise adjustment in the early design stage of air outlets. In this paper, we develop a numerical model of a commercial slot diffuser to predict its transient acoustic properties. Moreover, the paper presents the verification of the model and analyzes its ability to derive noise reduction strategies.

## 2 Methodology

### 2.1 Slot diffuser geometry

Figure 1 depicts the investigated ceiling slot diffuser. Supply air enters the plenum box via a central inlet. A rotatable circular perforated plate at the inlet acts as a throttle damper that allows for possible volume flow equalization. In this study, the damper remains completely open. The supply air enters the room through two slots, each 1000 mm long and 20 mm wide. The guiding geometry of the diffuser consists of three fixed

* Corresponding author: lisa.krueger@eonerc.rwth-aachen.de

guiding elements and four adjustable flaps attached to these. Our paper investigates the operating mode when all flaps are oriented towards the center. In this case, the air exiting the diffuser attaches to the ceiling.

(a) (b)

**Fig. 1.** Total view of the investigated slot diffuser (a) and detailed view of the flow guide elements (b).

## 2.2 Numerical aeroacoustic model and evaluation setup

The simulation model is developed in *Simcenter STAR-CCM + 17.06.008* [4] while adhering to the slot diffuser's original geometry to ensure precise simulation of sound generation and propagation. To reduce the computational resources required, we omit the mechanical connecting components, as well as three mounting rails that connect the guide geometry to the plenum box. Additionally, we fill all holes, cavities, and areas of low flow activity behind the center guiding flaps.

Figure 2 depicts the model geometry. The slot diffuser is attached to the ceiling of a room with the dimensions of 4000 × 2500 × 750 mm. A lengthened inlet pipe ensures a homogeneous supply flow. The volume mesh consists of $61 \cdot 10^6$ unstructured polyhedral cells. To achieve precise resolution of geometric features, the resolution is down to $\Delta = 0.25$ mm close to the guiding geometry. We maintain an average resolution of $\Delta = 1.5$ mm in the plenum box. To resolve the boundary layer accurately, we apply seven prism layers with a total thickness of $\Delta_{\text{Prism}} = 2$ mm.

The air is modeled as incompressible gas with a constant density of $\rho =$ 1.184 kg/s, temperature of $T = 300$ K, dynamic viscosity of $\eta = 1.855 \cdot$Pa s, and a reference pressure of $p_{\text{ref}} = 101325$ Pa. The supply air is supplied through the inlet pipe, while all room walls, except for the ceiling, function as pressure outlets. Those pressure outlets completely absorb sound. For the remaining surfaces, the sound is entirely reflected.

To investigate the influence of flow velocity on the aeroacoustic properties of the diffuser, we conduct a study involving three different volume flow rates (refer to Table 1). Prior to the transient simulation, we compute a Reynolds Averaged Navier Stokes (RANS) stationary solution for the flow field. Although the initial consideration favors using the *k-ω* turbulence model to accurately capture wall effects, we opt for the *k -ε* turbulence model since our previous study [5] has demonstrated that the supply air does not attach to the ceiling with the *k-ω* model. The calculation of the steady-state solution involves a total of 4000 iterations.

The calculation of the transient flow field and the time-dependent acoustic parameters is done in a Large Eddy Simulation (LES). The utilized numerical acoustic method is derived from the Linearized Perturbed Compressible Equations (LPCE), initially introduced by Seo and Moon [6] and later reformulated by Piepiorka and Von Estorff [7]. The *Siemens STAR-CCM +* implementation [4] assumes an incompressible fluid flow and a constant speed of sound $c_0$ and solves the flow field for an acoustic potential $\phi^a$ (see equation (1)) as a function of time *t*, the noise source damping term $\tau$, and the incompressible pressure fluctuation $p^f_{\text{inc}}$. Acoustic properties such as acoustic pressure, velocity, or density can be derived from this acoustic potential.

$$\frac{D^2\phi^a}{Dt^2} - c_0^2\Delta\left(\phi^a + \tau\frac{\partial\phi^a}{\partial t}\right) - \frac{1}{\rho}\nabla\phi^a \cdot \nabla p^f_{\text{inc}} = -\frac{1}{\rho}\frac{Dp^f_{\text{inc}}}{Dt} \tag{1}$$

The discretized time step of $1 \cdot 10^{-5}$ s ensures that the Courant-Friedrichs-Lewy number (CFL) is below one. The convective flows are discretized by a third-order MUSCL upwind scheme (Monotonic Upstream-centered Scheme for Conservation Laws) in combination with the method of central differences. Due to the challenges associated with stabilizing high-order discretization methods and additional attention required for simulation quality [4], the transition from second to the more accurate third-order scheme and the application of the acoustic model start after 5000 time steps (0.05 s physical time). The maximum number of inner iterations is limited to 5.

A point located 50 mm below the exit plane in the central section of the air diffuser serves as a microphone for the acoustic pressure. We analyze the recorded signal by breaking it down into its spectral components using an algorithm by Welch [8] that computes the power spectral density (PSD). This approach, as opposed to the classic FFT method, minimizes the impact of noise [9]. While it may reduce the spectrum resolution, it facilitates the identification of isolated power peaks, enhancing the interpretability and comparability of the results.

To facilitate the comparison of frequency spectra between measurement and simulation we calculate the one-third octave band levels. Initially, we determine the lower, middle, and upper frequency limits of the bands according to DIN EN ISO 266 [10]. We implement a bandpass filter, utilizing a type 1 Chebychev filter of 6th order, characterized by a ripple of 0.005 dB and an attenuation of 50 dB at the stopband edges. Subsequently, we determine the sum level for each one-third octave band. Additionally, we calculate the overall level with a bandpass filter between 100 and 4000 Hz.

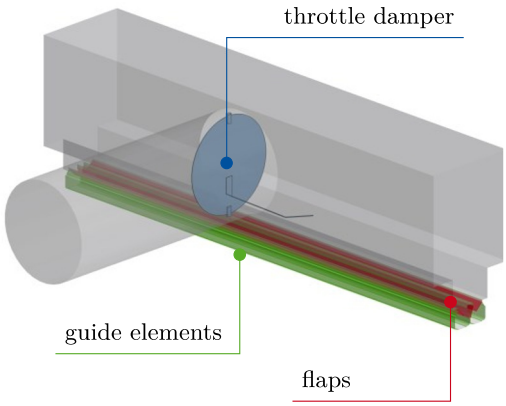


**Fig. 2**. Simulation model of the slot diffuser [5].

**Table 1.** Overview of the simulated volume flows and Reynolds numbers.

| Volume flow rate $m^3/h$ | Re |
|---|---|
| 182 | 5100 |
| 267 | 7700 |
| 351 | 10200 |

## 2.3 Experimental setup

For the acoustic measurements, the slot diffuser is installed in the center of a test chamber with the dimensions 4000 × 4000 × 3500 mm. The diffusor's exit opening faces upwards. Figure 3 depicts the experimental setup. A supply unit outside the test chamber supplies air into the plenum box. The suspended ceiling is equipped with sound-absorbing mineral wool panels, and absorber elements shield the inner walls of the measurement chamber. To further mitigate sound reflections, acoustic foam mats cover critical construction parts. These measures not only reduce the reverberation time but also diminish the transmission of external noise into the test chamber. Upon entering the measurement chamber, the supply air first passes through a silencer to reduce noise emitted by the supply unit. Metal ducts route the supply air to the plenum box, featuring a smooth inner surface to minimize turbulence and associated noise emissions. We avoid large diameter jumps in the design. An opening in the wall allows for the exhaust of air. In the experiment, we use two free-field microphones. One of these is located 1.5 m above the outlet at the center. The other one captures ambient noise outside the measuring chamber, accounting for the acoustic influence of the supply unit and the immediate environment of the test hall. Additionally, three *M352C68* acceleration sensors measure the structure-borne sound of the air diffuser (see Figure 3 *piezo x, y,* and *z)*. These sensors are located in the center of the outlet plane of the diffuser and on the long and short sides of the plenum box. We use a reference value of $9.81 \cdot 10^{-7}$ m/s$^2$ to determine the level values of the vibration measurements.

The acoustic experiment involves all three simulated volume flow rates (see Table 1). We conduct a baseline measurement by deactivating the air supply unit to accurately determine the noise emissions from the surrounding test hall environment. To further analyze the noise emitted by the supply unit, we measure the acoustic pressure signal of the supply unit without an installed air diffuser. In this measurement, the air is supplied directly into the chamber through the inlet pipe. The measurement duration is 10 seconds with a sampling rate of 50 kHz. We calculate the PSD using Welch's method with a window width of 10000 samples, yielding a frequency resolution of 10 Hz. Three measurements are conducted for each volume flow rate and then averaged.

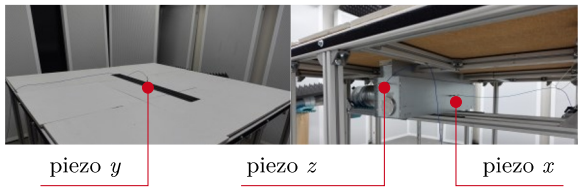


**Fig. 3**. Experimental setup of the acoustic measurements.

## 2.4 Implementation of geometric modifications

Our previous study on the emitted broadband noise of the slot diffuser [5] shows that the primary noise sources of the slot diffuser are the surfaces of the guiding geometry and the flaps. Hence, modifying the leading and trailing edges of the flow-guiding geometry presents a promising approach to noise reduction. The simulation model created for this study is particularly well-suited to serrations or a wave-shaped design of the flow profile edges since they can be easily implemented into the flow geometry. Nevertheless, it is crucial to avoid alterations that could limit the diffuser's functionality to optimize acoustic behavior. As the serrations on the trailing edges of flow significantly impact the flow profile directivity [11], we implement modifications on the leading edges of the outer guide elements. Figure 4 shows the implemented droplet-shaped modifications. Each element comprises a hemispherical front with a radius of $r_{\text{Element}} = 1.4$ mm and a cone with a total length of $l_{\text{Element}} = 10$ mm. The spacing between elements is 10 mm. We assess the effects of these alterations utilizing the same simulation setup as described in section 2.2.

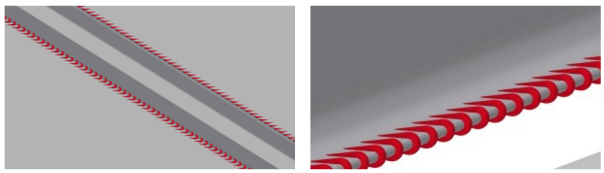

**Fig. 4**. Geometric modifications on the leading edge of the outer guide elements.

## 3 Results and Discussion

### 3.1 Solution of the transient flow field

Figure 5 displays the transient velocity field at $t = 0.3$ seconds on an $x$-$y$ and $x$-$z$ plane of the diffuser for a volume flow rate of $\dot{V} = 267$ m³/h. Upon entering the guiding geometry, both flaps direct the flow towards the central guide element, resulting in the flow velocity reaching the maximum in the area near the trailing edge of the flaps due to the deflection and narrowing of the cross-section. The flow is redirected at the leading edge of the central guide element and then enters the room on both sides at an angle of approximately 40 °. Coherent areas with increased mean velocity near the outlet in Figure 5(a) indicate the presence of vortex structures. These structures enable transverse movement and continually draw in more surrounding air so that the wall jet grows in the downstream direction.

The application of the $\lambda_2$-criterion [12] to the transient flow field confirms the presence of coherent structures. Figure 6(a) depicts large, coherent vortex structures present in the upper section of the plenum box, extending along the entire short side. The vortex core sizes here are approximately $d_V \approx 30$ mm. As the airflow progresses downstream towards the guiding geometry, the size of the vortex cores rapidly diminishes, indicating the breakdown into smaller coherent structures. The detailed view in Figure 6(b) illustrates the formation of small vortex structures with a vortex core diameter of approximately $d_V \approx 1$ to 2 mm at the trailing edge of the central guide element. These formations then expand and manifest as cohesive, larger vortex structures. The core diameter beneath the opening is roughly $d_V \approx 10$ mm. The previous study on broadband sound emission [5] revealed that solely the wall jet adjacent to the outflow is significant for aeroacoustics analysis. Here, the vortex pattern of the wall jet is predominantly irregular. However, isolated coherent vortex cores similar to horseshoe vortices can be identified (see Figure 6(b)). The wavelength of the emitted sound is dependent on both the local Mach number and the characteristic length of the coherent structures [13]. Since the sizes of the vortex core diameters and the geometric dimensions of the coherent vortex cores vary greatly, it is reasonable to assume that the sound signal has a broadband character. The omission of struts in the plenum box during the simulation constrains the analysis of the $\lambda_2$-criterion. Consequently, it is not possible to analyze the potential interactions between the coherent structures and the struts.

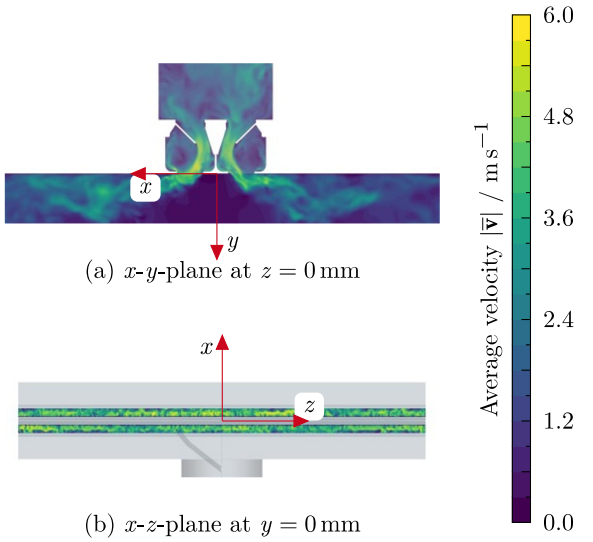


**Fig. 5.** LES velocity field for $\dot{V} = 267$ m³/h at $t = 0.3$ s.

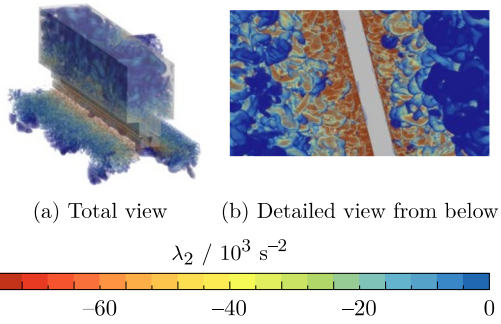


**Fig. 6**. Analysis of the $\lambda_2$-criterion for $\dot{V} = 267$ m³/h at $t = 0.3$.

### 3.2 LES results in combination with the acoustic pressure solution

The experimental setup for the acoustic measurements fails to meet the specifications of an anechoic chamber. To enable a precise result interpretation, we initially assess the potential acoustic interference from the test chamber's surroundings and the supply unit. Figure 7 presents the result of the spectral power density and one-third octave band levels (lines with markers) of the acoustic measurements for $\dot{V} = 267$ m³/h, the baseline, and the supply unit measurement.

The spectral analysis of the baseline noise measurement displays a pronounced peak at around 440 Hz. Smaller local maxima lie at around 200, 270, 300, and 330 Hz. These can also be identified in the acoustic measurement of the supply unit. This confirms that frequency components from the chamber environment influence the acoustic measurement of the diffuser in the low-frequency section. Between 600 and 900 Hz, the baseline noise PSD level rises, resulting in a corresponding increase in the PSD level of the supply unit and the diffuser. The impact of the surroundings in this frequency section is also apparent through the comparable trends of the averaged third-octave band levels. As there are no pronounced peaks evident in the frequency spectra of both the supply unit and baseline noise, it is possible to identify peaks originating from the diffuser in this frequency range. Above 1000 Hz, the

baseline noise PSD level significantly decreases, rendering the sound emission from the chamber environment negligible in this section.

Between 100 and 180 Hz and 600 to 900 Hz, the supply unit and baseline noise display similar PSD levels, implying low sound contribution from the supply unit. In the ranges 80 to 220 Hz, 260 to 380 Hz, and 600 to 900 Hz, the PSD level of the supply unit exceeds the baseline measurement with both curves showing a similar trend. This indicates a broadband sound emission from the supply unit. Clear peaks appear at around 230 Hz, between approximately 400 Hz, 960 Hz, and at 1300 Hz in the spectral analysis of the supply unit, but not in the baseline noise measurement, indicating noise emissions originating from the supply unit. Due to the decrease in the PSD level of the supply unit above 1600 Hz, the sound emission from the supply unit can be disregarded in this higher frequency range.

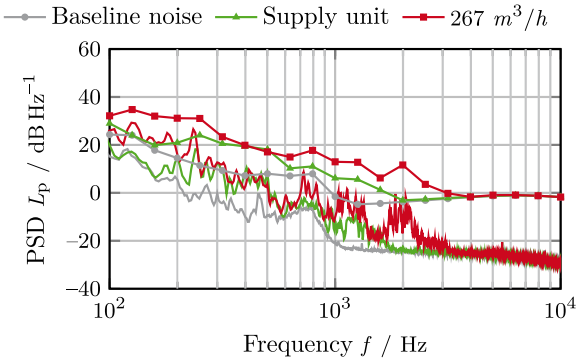


**Fig. 7.** Comparison of the frequency sprectra and one-third octave band levels (lines with markers) of the baseline noise, supply unit, and acoustic measurements for $\dot{V}$ = 267 m$^3$/h.

Figure 8 depicts the calculated spectral power densities and one-third octave band levels of the acoustic measurements. The corresponding PSD sum levels are presented in Table 2.

The frequency analysis shows a wide distribution of frequencies across the spectrum, demonstrating that the measured sound signal has broadband characteristics. The PSD level increases with higher volume flow rates or higher flow velocities, while the characteristics of the frequency spectra remain the same. The frequency spectra show a maximum near 130 Hz. A comparison of the results with the baseline measurement (see Figure 7) confirms that the pronounced peak around 230 Hz is due to the influences of the supply unit. The comparison also shows that the identification of local power peaks in the section between 230 and 600 Hz is challenging because of the superposition of local peaks from the chamber environment and the broadband signal from the diffuser. In the measurement series at flow rates of $\dot{V}$ = 267 m$^3$/h and 351 m$^3$/h, a local maximum occurs at a frequency of 600 Hz. The PSD significantly increases between 700 and 800 Hz. This heightened level is accompanied by three isolated peaks that cannot be attributed to either the environment or the supply unit. The initial analysis of acoustic influences due to the supply unit and environment indicates that within the range of 1000 to 1200 Hz, the PSD is notably influenced by the supply unit. Here, the PSD level of the diffuser for $\dot{V}$ = 267 m$^3$/h is approximately 5 to 10 dB/Hz higher than the supply unit's PSD level. Consequently, the measurement indicates that the diffuser emits more sound in this frequency range. Additionally, an increase in sound emission can be observed around the 2000 Hz frequency range. A comparison with the baseline measurement and the supply unit measurement (see Figure 7) shows that the influences from the supply unit and environment have no impact here. Two prominent peaks occur in the measurement series, with the highest volume flow rate in the high-frequency range, at around 5000 Hz and 6000 Hz. These peaks are less pronounced in the measurement series with lower flow velocities. The previous analysis of the sound emanating from the supply unit provides evidence that these discrete peaks in the high-frequency range can be ascribed to the air supply unit.

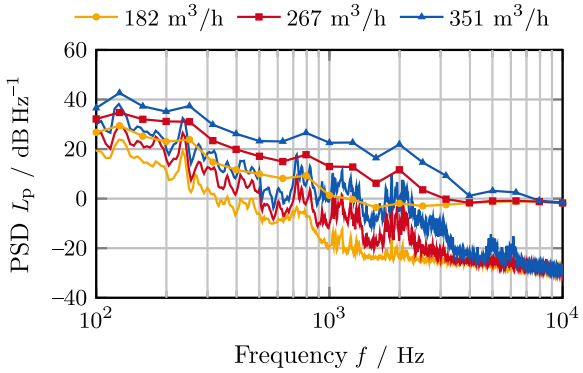


**Fig. 8.** Comparison of the frequency sprectra and one-third octave band levels (lines with markers) of the acoustic measurements for $\dot{V}$ = 182, 267, and 351 m$^3$/h.

**Table 2.** PSD sum levels of the acoustic measurements.

| $\dot{V}$ in m$^3$/h | 182 | 267 | 351 |
|---|---|---|---|
| PSD $L_{sum}$ in dB/Hz | 32.3 | 38.8 | 44.6 |

Based on the identified spectra characteristics, we discuss the results of the transient solution of the acoustic pressure. As we measure the sound pressure in the simulation at a point 50 mm below the outlet, whereas the free-field microphone captures the acoustic signal at a distance of 1500 mm from the diffusor exit plane, the sound pressure level in the simulation must be greater than in the measurement. Therefore, a direct comparison between the two levels is impossible. However, comparing the spectral analyses with regards to their characteristics allows for an assessment of the simulation's ability to predict the air diffuser's acoustic behavior. As pointed out earlier, the frequency spectrum characteristics remain constant while varying the flow velocity, hence we compare the simulation and experiment at a representative volume flow rate of $\dot{V}$ = 267 m$^3$/h. Figure 9 displays the frequency spectra and one-third octave band levels (lines with markers) of the measurement and the simulation. To aid in discussion, the spectral analysis also includes the acoustic measurement of the baseline noise.

The spectral analysis of the computed acoustic pressure signal demonstrates a wide distribution of

frequencies across the spectrum, indicating a broadband acoustic profile that agrees with the experimental measurements. Similar to the measurement, the numerical computed acoustic pressure level in the low-frequency range, approximately 100 to 200 Hz, is at a high level. However, the peak at 130 Hz is indistinct, potentially due to the small, analyzed time interval of 0.25 s allowing for 32 complete periods of a signal with a frequency of 130 Hz to be covered. Consequently, the simulation's resolution my not be sufficient to depict the distinctive characteristics. Beyond 200 Hz, the sound pressure decreases to a local minimum around 580 Hz. This minimum is both evident in the simulation and the measurement. The same applies to the local maximum at 600 Hz and the increase in PSD between 700 and 800 Hz. The similar behavior of the one-third octave band levels below 1000 Hz also demonstrates the successful prediction of the aeroacoustic behavior. However, above 1000 Hz, noise increasingly impedes the interpretation of the acoustic pressure. Unlike the measurement, the peak at 1100 Hz is shifted to slightly higher frequencies, with the PSD level measured being higher than that computed. Either the model cannot predict the sound pressure level in this section, or the experiment's interference sources have too much influence. The same complication arises in the frequency range surrounding 2000 Hz. Spectral analysis of the structure-borne sound emitted by the air diffuser during a parallel series of tests reveals that the high-frequency range measurements cannot be compared with the simulated sound pressure signal. The findings suggest that the power peaks observed at 2000 Hz in the acoustic measurement are not attributable to the aeroacoustics of the air diffuser but to ö

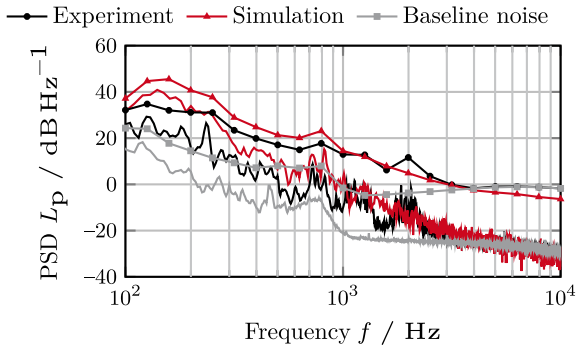


**Fig. 9.** Comparison of the frequency spectra and one-third octave band levels (lines with markers) of the acoustic measurements and LES for $\dot{V}$ = 267 m³/h.

### 3.3 Evaluation of the influence of geometric modifications

The transient calculation results in a total PSD level of 49 dB/Hz for the modified geometry, corresponding to an insignificant increase of 0.7 dB/Hz compared to the original geometry. Figure 10 depicts the analysis of the frequency spectra. The PSD in the low-frequency band persists at a high level. The power peaks at 700 Hz and 800 Hz, as well as at 1000 Hz and 1100 Hz, are still evident. The spectrum shows the same characteristics as described in section 3.2, indicating that the acoustic characteristics remain predominantly unaltered. The power peaks at 1000 Hz and 1100 Hz exhibit a slightly increased level in the modified simulation (≈ +5 dB/Hz) as compared to the original geometry. However, there is no discernible trend in the low-frequency range. A possible explanation for this could be the limited time resolution in this area as well as the rather small geometric extent of the modifications.

It is essential to extend the simulated time span to improve the validity of this result. But, considering the substantial computational resources required for these numerical calculations (81500 core-h per 0.25 s physical time calculated), the extension of the simulated time interval should be carefully evaluated with economic considerations. Furthermore, a thorough analysis of the transient flow phenomena surrounding the guide geometry is required to make definitive statements regarding specific peaks in the frequency spectrum.

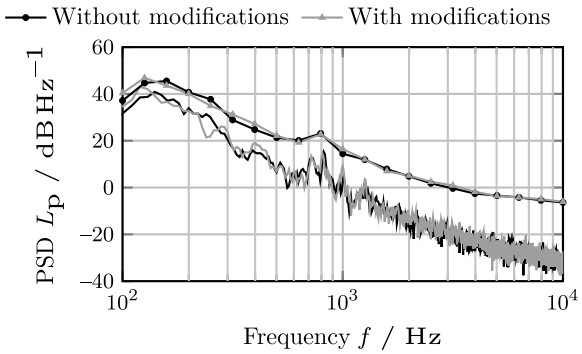


**Fig. 10.** Comparison of the simulated frequency spectra and one-third octave band levels (lines with markers) before and after geometric modifications for $\dot{V}$ = 267 m³/h.

## 4 Conclusion

This paper presents a numerical model for predicting the aeroacoustic behavior of a slot diffuser. The comparison between the experiment and simulation demonstrates that the simulation model, coupled with the LPCE-based approach, can predict the acoustic behavior of the diffuser, in terms of the emitted frequency spectrum. However, limitations arise from the low resolution within the low-frequency range due to the short, computed time interval. Extending the computed time interval is necessary for evaluating low frequencies, but the additional information gained must be weighed against the significant increase in computational cost for the transient calculation.

Moreover, structure-borne noise effects hinder the validation in the higher frequency range (1000 to 2000 Hz). The simulation results are also influenced by disregarded struts within the plenum box. Neglecting these struts and the interactions between these structures, the free flow, and the surfaces of the diffuser potentially leads to deviations in the frequency spectrum.

The introduction of geometric modifications highlights that even minor alterations impact the frequency spectrum of the air diffuser. Achieving noise reduction necessitates a detailed analysis of the flow

processes at the modifications and an iterative optimization of their geometry.

## Acknowledgement

Grateful acknowledgement is made for financial support by the Federal Ministry for Economic Affairs and Climate Action (BMWK), the DLR-Projektträger (DLR-PT) and the "Forschungsvereinigung für Luft- und Trocknungstechnik (FLT) e.V.", promotional reference 21611 N.
The authors gratefully acknowledge the computing time provided to them at the NHR Center NHR4CES at RWTH Aachen University (project number p0020083). This is funded by the Federal Ministry of Education and Research, and the state governments participating on the basis of the resolutions of the GWK for national high-performance computing at universities (www.nhr-verein.de/unsere-partner).

## References

1 German Federal Ministry for Housing, Urban Development and Building. *Gebäudeenergiegesetz*. GEG. (established on 8th August 2020 and updated on 16th October 2023).

2 C. Doolan, D. Moreau. *Flow Noise: Theory* (2022).

3 M. Tautz. *Aeroacoustic Noise Prediction of Automotive HVAC Systems*. Doctoralthesis.

4 *Simcenter StarCCM+ Documentation: Version 2022.1.1*.

5 P. Ostmann, L. Krüger, M. Kremer, D. Müller. *Contribution of Geometric Features on the Aeroacoustic Behaviour of a Slot Diffuser*. 36th International Conference on Efficiency, Cost, Optimization, Simulation and Environmental Impact of Energy Systems, ECOS (2023).

6 J. H. Seo, Y. J. Moon. *Linearized perturbed compressible equations for low Mach number aeroacoustics*. Journal of Computational Physics. **2**. 702–719 (2006).

7 J. Piepiorka, O. von Estorff. *Numerical Investigation of Hydrodynamic/Acoustic Splitting Methods in Finite Volumes including Rotating Domains*. Proceedings of the 23rd International Congress on Acoustics. 1827–1834 (2019).

8 P. Welch. *The use of fast Fourier transform for the estimation of power spectra: A method based on time averaging over short, modified periodograms*. IEEE Transactions on Audio and Electroacoustics. **2**. 70–73 (1967).

9 T. P. Zielinski. *Starting Digital Signal Processing in Telecommunication Engineering* (2021).

10 *Akustik - Normfrequenzen DIN EN ISO 266*.

11 B. Lyu, M. Azarpeyvand, S. Sinayoko. *Prediction of noise from serrated trailing edges*. Journal of Fluid Mechanics. 556–588 (2016).

12 J. Jeong, F. Hussain. *On the identification of a vortex*. Journal of Fluid Mechanics. 69–94 (1995).

13 S. Schoder, M. Kaltenbacher. *Hybrid Aeroacoustic Computations: State of Art and New Achievements*. Journal of Theoretical and Computational Acoustics. **04**. 1950020 (2019).